Adhesive-based tendon-to-bone repair: failure modeling and materials selection

Evangelos I. Avgoulas[1], Michael P. F. Sutcliffe[1], Stephen W. Linderman[2], Victor Birman[3], Stavros Thomopoulos[4], Guy M. Genin[5*]

Affiliations:

1. Department of Engineering, University of Cambridge, Trumpington Street, Cambridge CB2 1PZ, UK

2. Department of Orthopaedic Surgery, Washington University School of Medicine, St. Louis, MO 63131, USA

3. Missouri Science & Technology Global-St. Louis, and Department of Mechanical and Aerospace Engineering, St. Louis, MO 63131, USA

4. Department of Orthopedic Surgery, Department of Biomedical Engineering, Columbia University, New York, NY 10032, USA

5. NSF Science and Technology Center for Engineering Mechanobiology, Department of Mechanical and Aerospace Engineering, Washington University, St. Louis, MO 63130, USA

Corresponding author:

* Guy M. Genin, NSF Science and Technology Center for Engineering Mechanobiology, Department of Mechanical Engineering and Materials Science, Washington University, St. Louis, MO 63130, USA. genin@wustl.edu

Adhesive-based tendon-to-bone repair:
failure modeling and materials selection

Abstract

Surgical reattachment of tendon to bone is a procedure marked by high failure rates. For example, nearly all rotator cuff repairs performed on elderly patients with massive tears ultimately result in recurrence of tearing. These high failure rates have been attributed to stress concentrations that arise due to the mechanical mismatch between tendon and bone. Although recent studies have identified potential adhesives with mechanical properties tuned to alleviate these stress concentrations and thereby delay the onset of failure, resistance to the progression of failure has not been studied. Here, we refined the space of adhesive material properties that can improve surgical attachment by considering the fracture process. Using cohesive zone modeling and physiologically relevant values of mode I and mode II adhesive fracture toughnesses, we predicted the maximum displacement and strength at failure of idealized, adhesively bonded tendon-to-bone repairs. Repair failure occurred due to excessive relative displacement of the tendon and bone tissues for strong and compliant adhesives. The failure mechanism shifted to rupture of the entire repair for stiffer adhesives below a critical shear strength. Results identified a narrow range of materials on an Ashby chart that are suitable for adhesive repair of tendon to bone, including a range of elastomers and porous solids.

Key words: Enthesis, rotator cuff, cohesive zone model

Introduction

Injuries at or near the attachment of tendon to bone (the “enthesis”), e.g., rotator cuff tears, heal poorly and often have poor surgical outcomes. These injuries are a widespread problem, with approximately half of the US population over 60 years old having a rotator cuff tear [1]. Surgical repair techniques, such as the double-row suture bridge approach, improve reattachment by compressing the tendon to its footprint [2], but nevertheless concentrate force where sutures grasp the tendon (Fig. 1). Recurrence of tearing at the healing interfaces after surgical repair is as high as 20% in healthy adults with small tears and 94% in older adults with massive tears [3–5]. Many of these failures of surgical repair occur within the first few weeks post-surgery and are associated with stress concentrations at the suture grasping points and at the tendon-to-bone bi-material interface [6,7][8] or from vascular constriction associated with over-tensioned sutures [2].

Recent engineering efforts to improve surgical repair of tendon to bone have focused on replicating the types of energy absorption mechanisms present in the healthy attachment. While the initiation of failure is believed to be resisted by stress-reducing mechanisms such as functional material and spatial grading [9,10], the resistance to failure is thought to be mediated by mechanisms that maximize the volume of tissue structures that absorb energy across hierarchies during failure [11,12]. For example, the enthesis reduces stress concentrations by distributing force over a footprint that is large compared to the tendon diameter and by redistributing stresses through a compliant transitional fibrocartilaginous zone [13–19]. In response to injury-level stresses, this compliant zone absorbs energy through a range of mechanisms, such as

mineral sliding, that employ disorder and heterogeneity to distribute stresses over a larger volume [20,21].

Technologies such as adhesive sutures and films have been proposed to reduce stress concentrations and thereby increase the strength at which failure begins [6,7]. Although no adhesive repair systems are current approved for tendon-to-bone healing by the US Food and Drug Administration, several adhesives with tailored combinations of strength and modulus appear to be promising candidates. Given a range of acceptable strength and modulus, the classes of materials that could meet the mechanical requirements needed for improved resistance to the onset of failure can be identified on an Ashby chart [6,7]. Ashby charts plot the entire set of known materials on typically logarithmic axes representing their property ranges and thereby facilitate materials selection [22]. After removing materials that obviously unsuitable for surgical repair because of their toxicity or bio-incompatibility, a range of candidate materials remain including porous several polymeric foams and elastomers, including natural elastomers such as DOPA-based adhesives [23,24].

However, the strength and ductility of such adhesive-based repairs have not been evaluated. The ultimate load and ultimate displacement of an adhesive repair depend not only upon initiation of failure, but upon the ways that the structure and the adhesive interact over the course of failure. A successful adhesive repair must prevent the tendon from displacing so far from the bone that tissue integration is disrupted, and must not introduce so much ductility into the repair as to impair the functioning of the joint. Additionally, the failure load must be sufficiently high to prevent rupture of the adhesive. Therefore, to assess how adhesive modulus and strength affect mechanical functioning

of the enthesis over the course of failure, we performed a series of simulations of an idealized repair, with adhesive failure modeled using a cohesive zone approach. The cohesive zone modeling approach simulated the gradual degradation of material properties over the course of failure. We combined this with earlier analyses of enthesis mechanics to identify a range of adhesives that can both strengthen and toughen the attachment site when used to augment the surgical repair.

Methods

Finite element model and discretization

Two-dimensional (2D) finite-element models of a tendon-to-bone repair configuration (Figure 1) were developed within the finite element software ABAQUS 6.12 (Dassault Systèmes, Vélizy-Villacoublay). In the 2D plane strain model, a rectangular, isotropic tendon was attached to a smooth, isotropic, rectangular bone by an adhesive applied over an overlap length of 13 mm. Physiologically relevant dimensions were chosen: the bone and tendon free lengths were equal to 26 mm and 75 mm, respectively; The thickness of the bone and tendon were equal to 7.5 mm and 2 mm, respectively; and, the thickness of the adhesive was equal to h = 0.5 mm.

Linear 4-node incompatible-modes bilinear plane strain quadrilateral elements (Abaqus element type CPE4I) were used for both tendon and bone adherends. The mesh density was chosen to ensure convergence and accuracy for the model. Standard mesh refinement tests were performed to ensure that the predicted displacements did not change more than 3% with further refinement. We note that predictions using cohesive

elements are notoriously mesh-dependent and can lead to highly divergent crack paths. The mesh was therefore designed to ensure that the failure process zone stayed within the adhesive layer. Convergence was achieved with 8477 identically sized, square elements in the model.

To estimate the load-carrying capacity of the repairs, standard cohesive elements were used for the simulation [25]. The adhesive was modelled with a single layer of 4-node, two-dimensional (2D) cohesive elements (COH2D4) of thickness 0.5 mm, compatible with the CPE4I elements used for the tendon and bone adherends [26].

Parametric analysis of material properties

As a first approximation, the bone and tendon adherends were modeled with isotropic material properties. The Young's modulus of the bone substrate was taken as 20 GPa and the Poisson's ratio as 0.3 [10]. The Young's modulus of the tendon adherend was taken as 200 MPa and the Poisson's ratio as 0.2 [27].

Cohesive zone model

The deformation and fracture of the adhesive was modeled using a triangular cohesive zone degradation formulation, as is commonplace for brittle adhesives [28]. For loading in the opening direction, the traction-separation law was triangular with opening displacement $\delta_n = 0$ for normal traction $t_n \le 0$, and for $t_n \ge 0$,

$$t_n = \begin{cases} E\delta_n / h, & 0 \le \delta_n \le \delta_n^o \\ \dfrac{E\delta_n^o}{h}\left(\dfrac{\delta_n^{\max} - \delta_n}{\delta_n^{\max} - \delta_n^o}\right), & \delta_n^o \le \delta_n \le \delta_n^{\max} \\ 0, & \delta_n \ge \delta_n^{\max} \end{cases} \quad (1)$$

where E and h are the elastic modulus and thickness of the adhesive layer, respectively; $\delta_n^o = \sigma_f^o h / E$ is the displacement associated with the onset of strain softening and the peak traction σ_f^o; and δ_n^{max} is the displacement beyond which the interface can bear no further load. A similar relation was applied in pure shear in axes normal and parallel to the adherends, except that the relation was symmetrical for positive and negative shearing:

$$t_s = \begin{cases} 0, & \delta_s \le -\delta_s^{max} \\ -\dfrac{\mu\delta_s^o}{h}\left(\dfrac{\delta_s^{max}+\delta_s}{\delta_s^{max}-\delta_s^o}\right), & -\delta_s^{max} \le \delta_s \le -\delta_s^o \\ \mu\delta_s / h, & -\delta_s^o \le \delta_s \le \delta_s^o \\ \dfrac{\mu\delta_s^o}{h}\left(\dfrac{\delta_s^{max}-\delta_s}{\delta_s^{max}-\delta_s^o}\right), & \delta_s^o \le \delta_s \le \delta_s^{max} \\ 0, & \delta_s \ge \delta_s^{max} \end{cases} \quad (2)$$

where t_s and δ_s are shear traction and displacement, respectively; μ is the adhesive shear modulus; $\delta_s^o = \tau_f^o h / \mu$ is the displacement associated with the onset of strain softening and the ultimate adhesive shear stress τ_f^o; and δ_s^{max} is the displacement beyond which the interface can bear no further load. The material properties used to define the cohesive law are summarized in Table 1.

A broad range of fracture criteria exist that represent how adhesives respond to a combination of normal and shear loadings [29]. We adopted a simple quadratic nominal stress criterion to define the mixed mode ultimate cohesive strength:

$$\left(\frac{\langle t_n \rangle}{\sigma_f^o}\right)^2 + \left(\frac{t_s}{\tau_f^o}\right)^2 = 1 \qquad (3)$$

where the Macaulay brackets, ⟨ ⟩, emphasize that a purely compressive normal stress does not initiate fracture.

After this criterion was satisfied, the traction versus separation law adopted a negative slope, so that the isometric force for further extension reduced. For consistency amongst simulations, the opening and shearing fracture energies (G_{IC} and G_{IIC}, respectively) were held constant for all materials, and the moduli E and μ and the ultimate shear strength τ_f^o were varied parametrically. Because tensile separation of the surfaces is substantially more of an impediment to healing than excessive shearing, the tensile strength σ_f^o was set to a reasonable lower limit of τ_f^o; note that for an isotropic material σ_f^o is often twice τ_f^o. Then, for a particular value of τ_f^o the parameters δ_s^{max} and δ_n^{max} were calculated from:

$$\delta_n^{max} = \frac{2G_{IC}}{\sigma_f^o} \qquad \delta_s^{max} = \frac{2G_{IIC}}{\tau_f^o} \qquad (4)$$

This criterion placed limits on the maximum possible crack tip opening displacement for prescribed values of G_{IC}, G_{IIC}, τ_f^o, and σ_f^o: the cohesive law became brittle (no post-yield deformation) when the $\delta_n^{max} \le \delta_n^*$ or $\delta_s^{max} \le \delta_s^*$, where δ_n^* and δ_s^* are the values of δ_n where δ_s that satisfy the yield criterion, Equation (4):

$$\left(\frac{E\left\langle\delta_n^*\right\rangle}{h\sigma_f^o}\right)^2+\left(\frac{\mu\delta_s^*}{h\tau_f^o}\right)^2=1 \tag{5}$$

For the case of uniaxial tension, this yields a dimensionless criterion for brittle behavior:

$$\frac{h\left(\sigma_f^o\right)^2}{2G_{IC}E}\geq 1 \tag{6}$$

In the case of pure shear, an analogous criterion arises:

$$\frac{h\left(\tau_f^o\right)^2}{2G_{IIC}\mu}\geq 1 \tag{7}$$

Additionally, the fracture can become brittle when the strain energy stored in the tendon prior to satisfying Equation (3) is large compared to G_{IC} and G_{IIC}. For any material points at which crack opening displacement reduced prior to complete failure of that material point, the force reduced linearly to zero and then returned along that same path in reloading.

Solution of equations

A geometrically non-linear static general analysis was performed in Abaqus/Standard. Fixed boundary conditions were applied to the bone end of the repair together with restriction of bending in the bone free length area. A horizontal displacement, u_x, was applied to the tendon end of the model.

Results and Discussion

In a typical simulation, a stress concentration was evident at the loaded free edge of the adhesive layer at lower loading levels, as seen in contour plots of normalized strain energy density (Figure 2). This stress concentration moved away from the free edge as loading progressed and the portions of the adhesive that had failed became more compliant (Figure 2). At failure in a well-tuned adhesive, the peak concentration of strain energy moved to the opposite end of the adhesive layer (Figure 2).

The force-displacement curves for such a case (Figure 3) showed nonlinearity during the rise to a peak loading force, followed by a nearly linear decline in force with increasing displacement. The peak force increased with the shear strength of the adhesive for a fixed adhesive modulus and fixed fracture energies. Nonlinearity in the force-displacement curve was evident due to the initiation of failure in the adhesive being attenuated by its energy absorptive capacity. Nonlinearity was more pronounced at intermediate levels of shear strength. For fixed shear strength and shear modulus, the peak force and displacement at failure increased with increasing fracture toughness of the adhesive (Figure 4).

The effect of shear strength was strong compared to the effect of varying fracture toughness (Figures 3 and 4). Varying fracture toughness over an order of magnitude led to a less than doubled peak load and less than doubled peak displacement. We therefore used characteristic values of fracture toughness and focused on quantifying the effects of adhesive shear strength and modulus on repair performance. In all subsequent simulations, G_{IC} = 200 J/m^2 and G_{IIC} = 350 J/m^2 were therefore used.

The failures observed in the simulations fell into three distinct failure mechanisms. Two of these related to excessive displacement. The first was the displacement Δ of the end of the tendon which, if excessive, renders the repaired site incapable of transferring sufficient force for physiological functioning of the shoulder. We took the upper limit of acceptable tendon displacement Δ_{ult} as 6 mm during physiological loading. Even for adhesives intended only for the initial stages of healing when re-tearing is most likely to occur, the reduced muscle loading associated with failure through this criterion can be expected to be detrimental.

The second failure mechanism was what we termed excessive "extensometer displacement," δ. If the peak displacement of the tendon relative to the bone is excessive, tissue integration can be impaired. We set the upper limit of extensometer displacement δ_{ult} as 500 μm. Note that the ultimate extensometer displacement is smaller than the tendon displacement at a particular loading level due to the elastic stretching of the tendon.

Finally, we explored a failure mechanism in which the adhesive failed before the tendon achieved a physiologically relevant load. The threshold for this was set at 20 N of load on the tendon.

The first failure mechanism explored was that of ultimate tendon displacement at failure, Δ (Figure 5). Failure displacement increased with shear strength of the adhesive, and increased with shear modulus of the adhesive up to $G \approx 1$ MPa. The criterion of $\Delta \leq 6$ mm was not exceeded for any of the combinations of adhesive shear strength and adhesive shear modulus tested.

However, due to the constraints on the prospective materials being tested, a portion of material parameter space was inaccessible, and this provided the first constraint for material selection. The elastic displacement limits δ_n^o and δ_s^o for the adhesive had to be less than δ_n^{max} and δ_s^{max} in extension and shear, respectively, to avoid brittle failure. Approximations for this come from Equations (4). As an example, for the conditions used in this study, if the maximum stress before the adhesive became brittle was dictated by the shear case, the possible materials would have to satisfy $\left(\tau_f^o\right)^2 \big/ G \leq 1.4$ MPa. The inaccessible material space was denoted in Figure 5a via gray shading. Superimposing this upon an Ashby plot [22] of materials shows that a range of elastomers, foams, and structured materials such as honeycombs meet this criterion (Figure 5b).

The design space was further refined by considering the limit on extensometer displacement δ at failure (Figure 6). The displacement δ increased with decreasing adhesive shear modulus and increasing shear strength (Figure 6a). Superimposing the limit of $\delta \leq 0.5$ mm onto the Ashby plot of Figure 5b further reduced the space of suitable materials, eliminating a range of foams and elastomers (Figure 6b). This latter constraint was needed to ensure that the tendon and bone tissue initially adjoining each other would not slip so far as to negatively affect healing.

The final mechanism considered was failure strength for the repair. Isoclines of constant strength showed that failure strength of the adhesive repair increased with the adhesive strength (Figure 7a). Enforcing the need for a minimum repair strength of 20 N

eliminated weaker foams and honeycombs from the set of suitable materials, but did not reduce the space of suitable elastomers (Figure 7b).

The final design space suggested a range of materials that can be suitable candidates for an intermediate layer between tendon and bone. This region of parameter space was smaller than that found previously considering only shear lag models of strength [7]. However, several materials were left as viable candidates to be the first adhesives used in surgical tendon-to-bone reattachment. The first material of note is tendon itself, which has a shear strength on the order of 1-10 MPa and a shear modulus on the order of 100 MPa. This suggests that if tendon could adhere directly to bone with perfect adhesion, it would be capable of a tough attachment. Also of note are materials that would have the appropriate properties but that are not suitable as adhesives, including cork and low density polyethlylene. The organophosphorus compounds such as tetrakis(hydroxymethyl)phosphonium chloride, a crosslinking agent that can stiffen and strengthen tendon, would be suitable. Additionally, adhesives such as the DOPA-based adhesives used by mussels are potential candidates, as are a range of other adhesives including epoxies if presented in a porous, foamed form. This suggests that a range of feasible adhesives exists that would be suitable for tendon-to-bone repair.

We conclude with three caveats. We first note that tendon was modeled as isotropic. This is a limitation of the model; however, because microstructural order and hence tissue anisotropy are attenuated in healing tissue at the tendon-to-bone insertion site [30], isotropy is likely a reasonable first order approximation for the case of an injured tendon being reattached to bone [10].

The second caveat is that we constrained the tendon to be loaded with a horizontal force that was not angled from the adhesive layer. This was appropriate because patients are typically restrained from lifting their elbows above their heads following rotator cuff surgery. To identify any cases in which an opening failure might have become a possibility for this loading, the normal failure stress in the adhesive was set equal its shear failure stress, rather than to twice its value as would be expected for an isotropic material. Even with this, an opening mode of failure was not observed in the simulations. However, we note that the benefit of immobilization in tendon and tendon-to-bone healing is not clear [31–33], and that these opening mode displacements must be considered in greater depth if an adhesive repair is to be combined with a post-surgical exercise regime.

The third caveat is that the 2D model problem studied here is highly idealized. The use of an adhesive in the absence of mechanical fasteners is not likely to occur in surgery. Rather, we anticipate using a scenario such as that depicted in Figure 1, in which sutures and suture anchors are applied in parallel with an adhesive. Our simulations thus present a lower bound on the repair strength and on the range of materials that might be suitable as adjuvant treatments for sutured surgical repair.

Conclusions

Reattachment of tendon to bone is a major challenge in surgical practice. Adhesives that assist sutures in providing stability to repairs over the first few weeks of healing have been suggested as a means of improving surgical outcomes [6,7]. A range of

adhesives has been shown previously to be capable of reducing stress concentrations and improving the stress distribution along a repair [6,7]. By accounting for failure, as was done here for the first time, we narrowed the range of candidate adhesive materials that might be appropriate for use in surgical repair of tendon to bone. We observed that an adhesive that is too compliant leads to excessive displacement across the attachment at failure, and an adhesive that is too weak leads to a lower failure load. An adhesive that is too stiff leads to amplification of stress concentrations, and also weakens the repair. However, with all of these factors accounted for through the simulations in this study, a broad range of materials on an Ashby chart were still left as candidates for surgical adhesives. Results suggest that surgical repair of tendon to bone can be substantially enhanced by adhesives.

Competing interests

Although we have no competing interests, we have applied for US patents on technology related to the approach studied in this article.

Authors' contributions

EIA carried out the numerical simulations; all authors participated in data analysis and participated in the design of the study; EIA and GMG drafted the manuscript; all authors edited the manuscript. All authors gave final approval for publication.

Data Accessibility

Matlab scripts to produce Figures 5, 6, and 7 in their entirety, including all finite element data for those figures, are available by email from the authors.

Funding Statement

This study was supported by the National Institutes of Health (NIH) through grants U01 EB016422 (to ST and GMG), R01 AR062947 (to ST), and F30 AR069491 (to SWL), and by an Engineering and Physical Sciences Research Council (EPSRC) Doctoral Prize awarded by the University of Cambridge to EIA.

Table 1. Properties of the adhesive.

Shear modulus, G (GPa)	Variable
Young's modulus, E (GPa)	$E = 2G(1 + v)$
Poisson's ratio, v	0.49
Shear ultimate strength, τ_f (MPa)	Variable
Tensile ultimate strength, σ_f (MPa)	$\sigma_f = \tau_f$
Mode I strain energy release, G_{IC} (J/m^2)	200
Mode II strain energy release, G_{IIC} (J/m^2)	350

References

[1] K. Yamaguchi, New guideline on rotator cuff problems, AAOS Now. 5 (2011). http://www.aaos.org/news/aaosnow/jan11/cover1.asp.

[2] N.S. Cho, B.G. Lee, Y.G. Rhee, Arthroscopic rotator cuff repair using a suture bridge technique is the repair integrity actually maintained?, Am. J. Sports Med. 39 (2011) 2108–2116.

[3] D.T. Harryman II, L.A. Mack, K.Y. Wang, S.E. Jackins, M.L. Richardson, F.A. Matsen III, Repairs of the rotator cuff. Correlation of functional results with integrity of the cuff., J Bone Jt. Surg Am. 73 (1991) 982–989.

[4] L.M. Galatz, C.M. Ball, S.A. Teefey, W.D. Middleton, K. Yamaguchi, The outcome and repair integrity of completely arthroscopically repaired large and massive rotator cuff tears., J Bone Jt. Surg Am. 86–A (2004) 219–224.

[5] E. Monaco, L. Labianca, A. Speranza, a M. Agrò, G. Camillieri, C. D'Arrigo, A. Ferretti, M. E., L. L., S. A., A. A.M., C. G., D. C., Biomechanical evaluation of different anterior cruciate ligament fixation techniques for hamstring graft, J. Orthop. Sci. 15 (2010) 125–131. doi:10.1007/s00776-009-1417-9.

[6] S.W. Linderman, I. Korompakis, R.H. Gelberman, V. Birman, U.G.K.K. Wegst, G.M. Genin, S. Thomopoulos, Shear lag sutures: Improved suture repair through the use of adhesives, Acta Biomater. 23 (2015) 229–239. doi:10.1016/j.actbio.2015.05.002.

[7] S.W. Linderman, M. Golman, T.R. Gardner, V. Birman, W.N. Levine, G.M. Genin, S. Thomopoulos, Enhanced tendon-to-bone repair through adhesive films, Acta Biomater. (2018). doi:10.1016/j.actbio.2018.01.032.

[8] C.A. Cummins, G.A.C. Murrell, Mode of failure for rotator cuff repair with suture anchors identified at revision surgery, J. Shoulder Elb. Surg. 12 (2003) 128–133. doi:10.1067/mse.2003.21.

[9] S. Thomopoulos, V. Birman, G.M. Genin, Structural interfaces and attachments in biology, Springer Science & Business Media, New York, NY, 2012. doi:10.1007/978-1-4614-3317-0.

[10] S. Thomopoulos, J.P. Marquez, B. Weinberger, V. Birman, G.M. Genin, Collagen fiber orientation at the tendon to bone insertion and its influence on stress concentrations, J. Biomech. 39 (2006) 1842–1851. http://www.sciencedirect.com/science?_ob=ArticleURL&_udi=B6T82-4GMS9G0-2&_user=8315259&_coverDate=12%2F31%2F2006&_rdoc=1&_fmt=high&_orig=search&_origin=search&_sort=d&_docanchor=&view=c&_acct=C000073987&_version=1&_urlVersion=0&_userid=8315259&md5=fe1edb0.

[11] Y. Hu, V. Birman, A. Deymier-Black, A.G. Schwartz, S. Thomopoulos, G.M.

Genin, Stochastic interdigitation as a toughening mechanism at the interface between tendon and bone, Biophys. J. 108 (2015) 431–437.

[12] G.M. Genin, S. Thomopoulos, The tendon-to-bone attachment: Unification through disarray, Nat. Mater. 16 (2017) 607–608. doi:10.1038/nmat4906.

[13] Y. Liu, A.G. Schwartz, V. Birman, S. Thomopoulos, G.M. Genin, Stress amplification during development of the tendon-to-bone attachment, Biomech. Model. Mechanobiol. 13 (2014) 973–983. doi:10.1007/s10237-013-0548-2.

[14] Y. Liu, V. Birman, C. Chen, S. Thomopoulos, G.M. Genin, Mechanisms of bimaterial attachment at the interface of tendon to bone, J. Eng. Mater. Technol. 133 (2011) 11006. doi:10.1115/1.4002641.

[15] F. Saadat, A.C. Deymier, V. Birman, S. Thomopoulos, G.M. Genin, The concentration of stress at the rotator cuff tendon-to-bone attachment site is conserved across species, J. Mech. Behav. Biomed. Mater. 62 (2016) 24–32. doi:10.1016/j.jmbbm.2016.04.025.

[16] B.E. Alexander, T.L. Daulton, G.M. Genin, J.D. Pasteris, B. Wopenka, S. Thomopoulos, The Nano-physiology of Mineralized Tissue, Proc. ASME 2009 Summer Bioeng. Conf. (2009). doi:10.1115/SBC2009-206616.

[17] G.M. Genin, A. Kent, V. Birman, B. Wopenka, J.D. Pasteris, P.J. Marquez, S. Thomopoulos, Functional grading of mineral and collagen in the attachment of tendon to bone, Biophys. J. 97 (2009) 976–985. doi:10.1016/j.bpj.2009.05.043.

[18] Y.X.X. Liu, S. Thomopoulos, V. Birman, J.-S.J.-S. Li, G.M.G.M. Genin, Bi-material attachment through a compliant interfacial system at the tendon-to-bone insertion site, Mech. Mater. 44 (2012) 83–92. doi:10.1016/j.mechmat.2011.08.005.

[19] B. Alexander, T.L. Daulton, G.M. Genin, J. Lipner, J.D. Pasteris, B. Wopenka, S. Thomopoulos, The nanometre-scale physiology of bone: steric modelling and scanning transmission electron microscopy of collagen--mineral structure, J. R. Soc. Interface. (2012) rsif20110880.

[20] P. V. Kolluru, J. Lipner, W. Liu, Y. Xia, S. Thomopoulos, G.M. Genin, I. Chasiotis, Strong and tough mineralized PLGA nanofibers for tendon-to-bone scaffolds, Acta Biomater. 9 (2013) 9442–9450. doi:10.1016/j.actbio.2013.07.042.

[21] J. Lipner, J.J. Boyle, Y. Xia, V. Birman, G.M. Genin, S. Thomopoulos, Toughening of fibrous scaffolds by mobile mineral deposits, Acta Biomater. (2017). doi:10.1016/j.actbio.2017.05.033.

[22] M.F. Ashby, Materials Selection in Mechanical Design, 4th Ed., Kidlington, Oxford: Butterworth-Heinemann, 2011.

[23] U.G.K. Wegst, M.F. Ashby, The mechanical efficiency of natural materials, Philos Mag. 84 (2004) 2167–2186. doi:10.1080/14786430410001680935.

[24] B.K. Ahn, S. Das, R. Linstadt, Y. Kaufman, N.R. Martinez-Rodriguez, R. Mirshafian, E. Kesselman, Y. Talmon, B.H. Lipshutz, J.N. Israelachvili, J.H. Waite, High-performance mussel-inspired adhesives of reduced complexity, Nat. Commun. 6 (2015) 7. doi:10.1038/ncomms9663.

[25] R.D.S.G. Campilho, M.D. Banea, J.A.B.P. Neto, L.F.M. Da Silva, Modelling adhesive joints with cohesive zone models: Effect of the cohesive law shape of the adhesive layer, Int. J. Adhes. Adhes. (2013). doi:10.1016/j.ijadhadh.2013.02.006.

[26] R.D.S.G. Campilho, M.F.S.F. de Moura, A.M.G. Pinto, J.J.L. Morais, J.J.M.S. Domingues, Modelling the tensile fracture behaviour of CFRP scarf repairs, Compos. Part B Eng. (2009). doi:10.1016/j.compositesb.2008.10.008.

[27] Y. Liu, S. Thomopoulos, C. Chen, V. Birman, M.J. Buehler, G.M. Genin, Modelling the mechanics of partially mineralized collagen fibrils, fibres and tissue, J. R. Soc. Interface. 11 (2014) 20130835. doi:10.1098/rsif.2013.0835.

[28] R.D.S.G. Campilho, M.D. Banea, A.M.G. Pinto, L.F.M. Da Silva, A.M.P. De Jesus, Strength prediction of single- and double-lap joints by standard and extended finite element modelling, Int. J. Adhes. Adhes. (2011). doi:10.1016/j.ijadhadh.2010.09.008.

[29] M. Charalambides, A.J. Kinloch, Y. Wang, J.G. Williams, On the analysis of mixed-mode failure, Int. J. Fract. (1992). doi:10.1007/BF00035361.

[30] S. Thomopoulos, Tendon to Bone Healing: Differences in Biomechanical, Structural, and Compositional Properties Due to a Range of Activity Levels, J. Biomech. Eng. (2003). doi:10.1115/1.1536660.

[31] S. Thomopoulos, E. Zampiakis, R. Das, M.J. Silva, R.H. Gelberman, The effect of muscle loading on flexor tendon-to-bone healing in a canine model., J Orthop Res. 26 (2008) 1611–1617. doi:10.1002/jor.20689.

[32] M.L. Killian, L. Cavinatto, S.A. Shah, E.J. Sato, S.R. Ward, N. Havlioglu, L.M. Galatz, S. Thomopoulos, The effects of chronic unloading and gap formation on tendon-to-bone healing in a rat model of massive rotator cuff tears., J Orthop Res. 32 (2014) 439–447. doi:10.1002/jor.22519.

[33] L.M. Galatz, N. Charlton, R. Das, H.M. Kim, N. Havlioglu, S. Thomopoulos, Complete removal of load is detrimental to rotator cuff healing, J. Shoulder Elb. Surg. 18 (2009) 669–675. doi:10.1016/j.jse.2009.02.016.

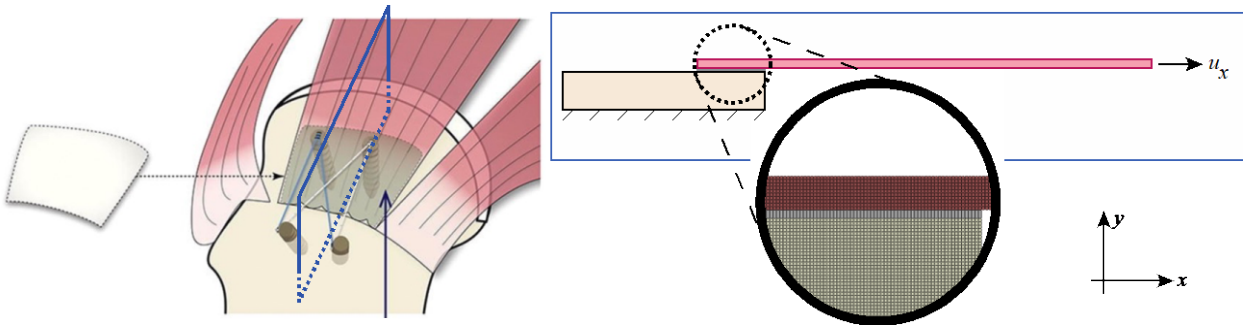

Figure 1. Two-dimensional finite-element models of a tendon-to-bone repair configuration were developed. On the left is shown a supraspinatus repair of the rotator cuff with an adhesive layer inserted. The cut represented by the blue box in the left panel was modeled using 2D, plane strain finite element analysis, as depicted by the schematic (red: tendon; tan: bone; light grey/green: adhesive with cohesive elements). Note that in a real repair, anchor screws such as the ones denoted by the blue arrow (left panel) would likely be used in addition to the adhesive patch. Quadrilateral elements were used for plane strain finite element analysis, with relatively high refinement in the vicinity of the adhesive.

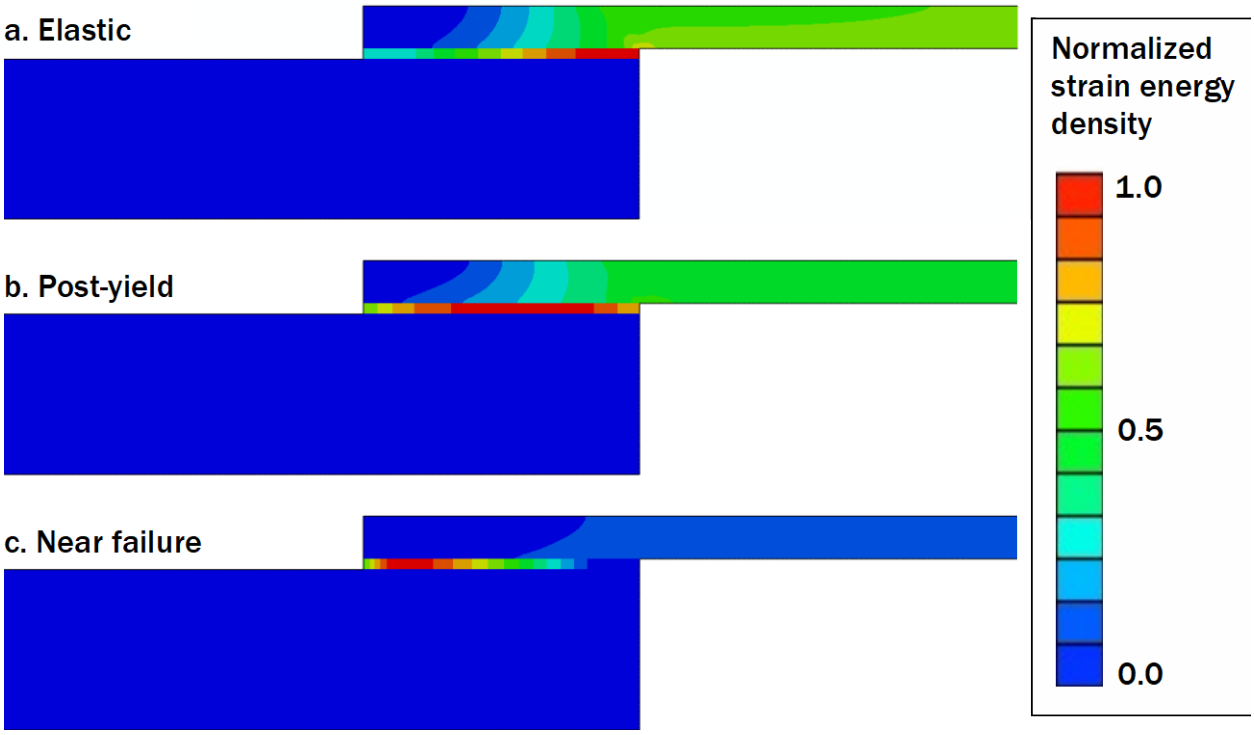

Figure 2. Contours of strain energy density over the course of a loading to failure, normalized by the peak strain energy density at each loading level. In this example, a concentration of strain energy was evident at the loaded end of the adhesive layer at lower loading levels (top panel). This concentration moved to the interior of the adhesive layer as the adhesive began to fail (middle panel), and translated to the left edge near final failure (bottom panel). Here, the adhesive layer had a shear modulus of 10 MPa and a shear strength of 1.4 MPa.

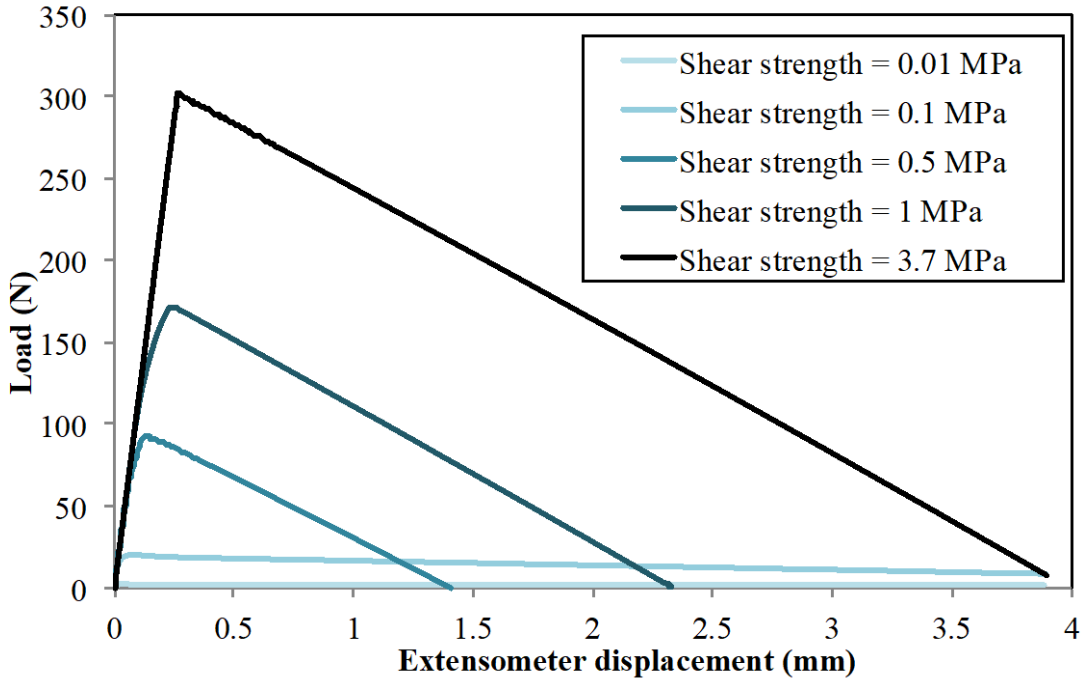

Figure 3. Force-displacement curves for displacement of an adhesive repaired tendon-to-bone enthesis. The mode I and mode II fracture toughnesses of the adhesive layer were set to G_{IC} = 200 J/m^2 and G_{IIC} = 350 J/m^2, respectively, and a shear modulus of 10 MPa was used.

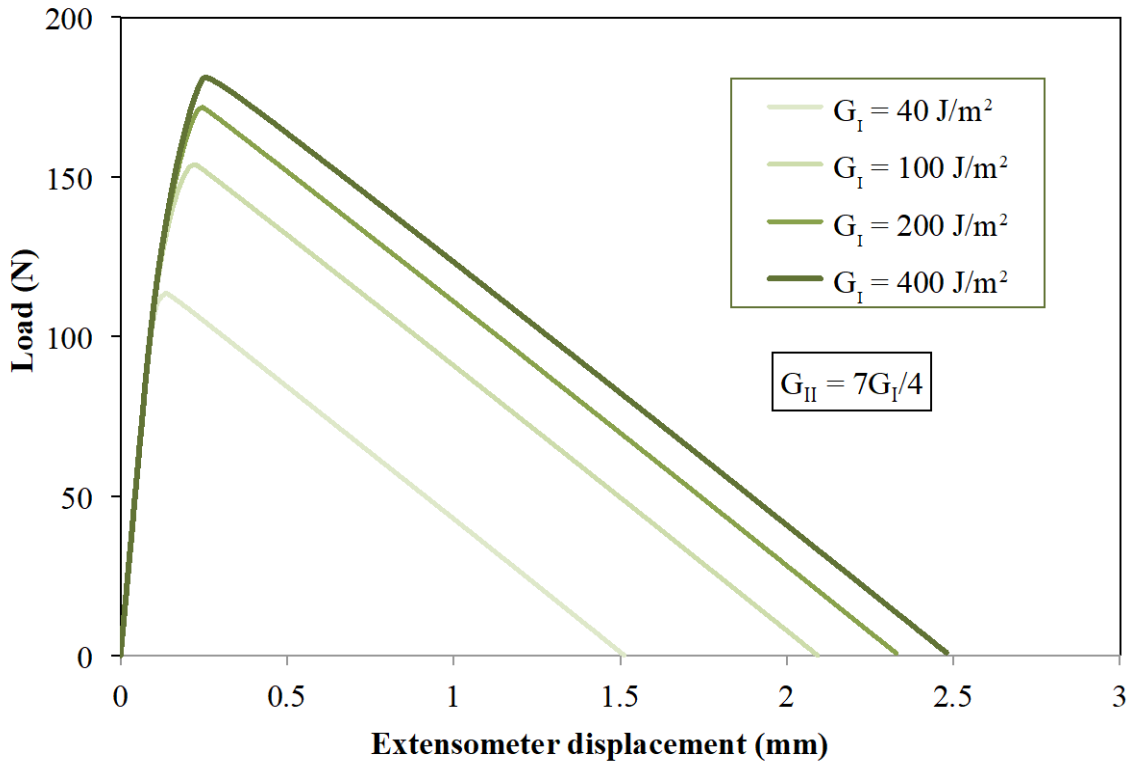

Figure 4. Force-displacement curves for displacement to failure of an adhesive repaired tendon-to-bone enthesis. The mode I and mode II fracture toughnesses were varied while a shear strength of 1 MPa and a shear modulus of 10 MPa were maintained.

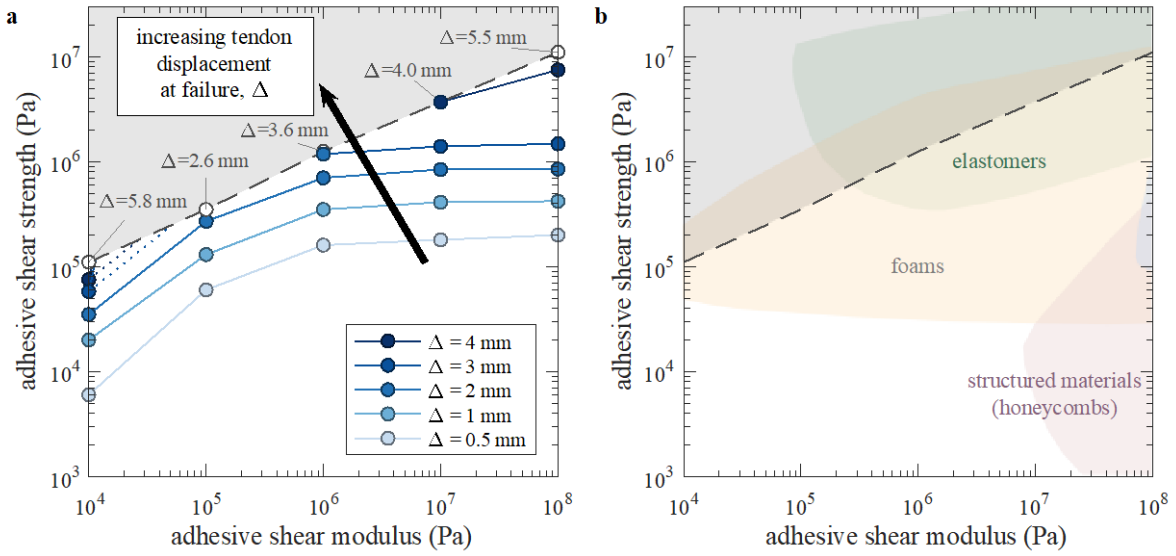

Figure 5. (a) Isoclines of constant tendon displacement at failure for G_{IC} =200 J/m^2 and G_{IIC} = 350 J/m^2, as a function of adhesive shear modulus and shear strength. The grey shaded region corresponds to the brittle limit: only materials for which $\left(\tau_f^o\right)^2 / G \leq 1.4$ MPa were admissible. (b) When superimposed upon an Ashby plot, a range of elastomers, foams, and structured materials such as honeycombs were revealed as meeting this criterion (i.e., the material space under the dashed line).

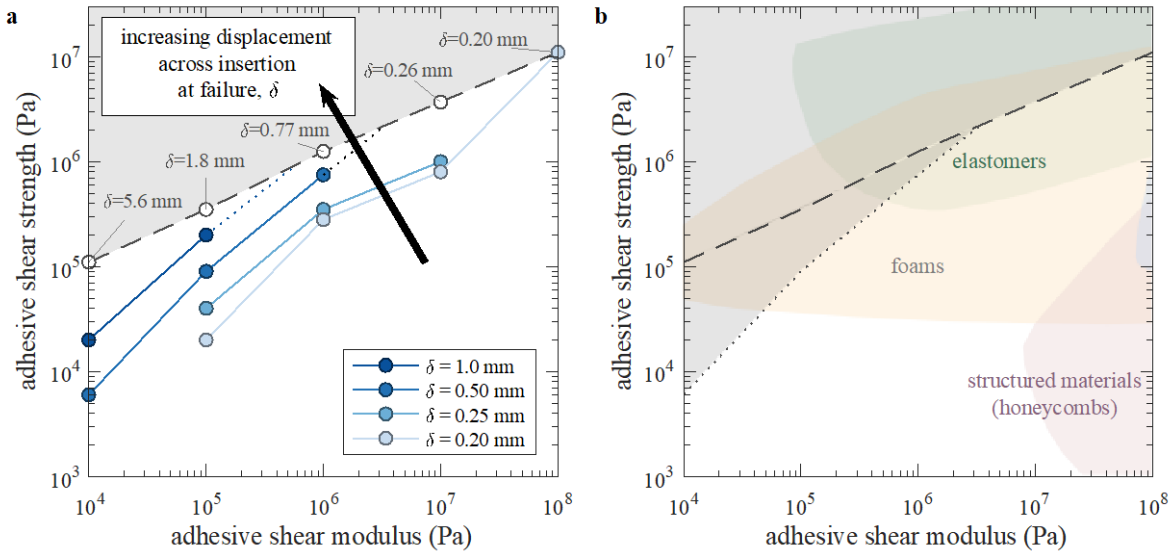

Figure 6. (a) Isoclines of constant "extensometer" displacement at failure for G_{IC} = 200 J/m^2 and G_{IIC} = 350 J/m^2, as a function of adhesive shear modulus and shear strength. (b) When the criterion of $\delta \leq 0.5$ mm was imposed, the range of suitable materials on the Ashby plot was further reduced (eliminated material space is indicated by the grey shaded region).

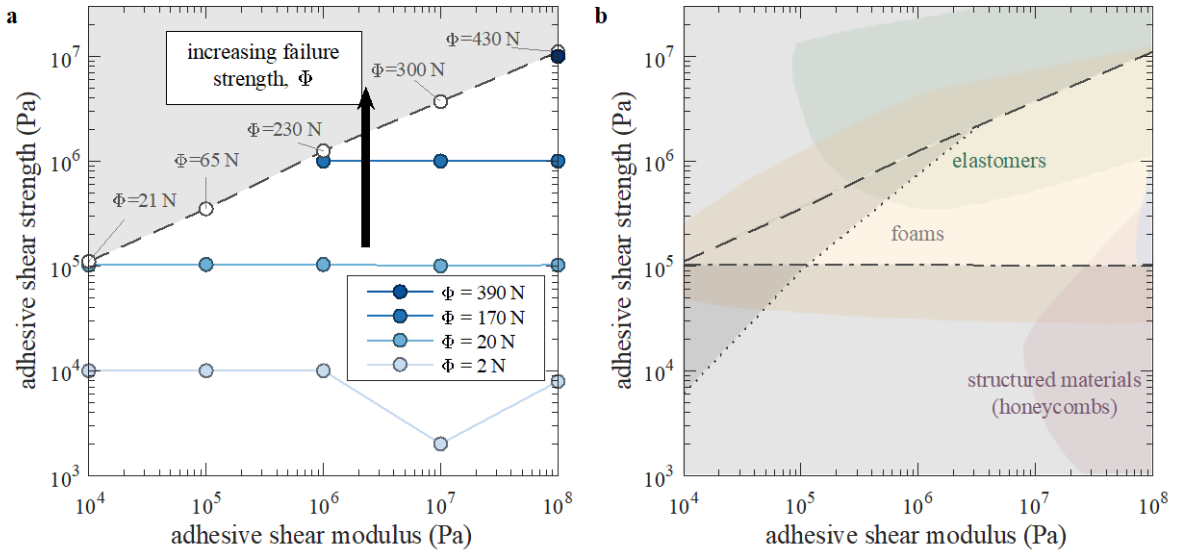

Figure 7. (a) Isoclines of constant repair strength showed that failure strength of the adhesive repair increased with the adhesive strength. (b) Enforcing a minimum repair strength of 20 N eliminated weaker foams and honeycombs from the set of suitable materials, but did not reduce the space of suitable elastomers. G_{IC} = 200 J/m^2 and G_{IIC} = 350 J/m^2 (eliminated material space is indicated by the grey shaded region).